scientific reports

Check for updates

OPEN

Neural network-based optimal and adaptable power allocation for real-time FSO-RF communications using Jetson nano

Mahdi Akbari[1], Saeed Olyaee[1,2]✉ & Gholamreza Baghersalimi[3]

Power allocation (PA) is a significant and challenging real-time optimization problem in the management of optical-radio wireless networks. Analytical methods involve numerous calculations and require an extended processing time. Therefore, DNNs are employed to design a fast, real-time PA system with the required accuracy. In this paper, the innovation of a real-time optimal PA system is presented, enabling two separate three-layer DNNs to perform FSO-RF PA in parallel. The WMMSE algorithm is utilized on various RF channel models, including fading and user priorities, to produce training data. Additionally, the analytical algorithm for calculating BER is used to adjust the transmitter power interval for different FSO channel models, accommodating various modulation schemes and transmitter and receiver sizes. Finally, the DNNs were implemented on Jetson Nano, and the results were compared and validated with analytical methods. The implemented system shows 1.6 Gbps for the sum rate and an average accuracy of 97.82% for the RF channel with 10, 20, and 30 users, while the FSO channel achieves 1.6 Gbps for the data rate and an average accuracy of 98.87%. The implemented system exhibits suitable accuracy and speed in comparison to analytical algorithms for real-time optimal PA in FSO-RF wireless networks.

Keywords Power allocation, FSO-RF wireless network, DNN, Optimization, Jetson nano

The growing need for data and the upgrade of future 5G wireless systems have become critical issues in wireless communication. Also, the need to use optical communication systems due to their wide bandwidth and high speed has always been of great importance. On the other hand, resource management and improving the total received rate in optical-radio wireless systems increase the data transfer speed[1–6]. Considering the cost-effectiveness of software methods in improving the management of optical wireless systems, researchers have long targeted the resource management system in wireless communication systems. The need for a comprehensive and optimal method for managing power consumption in optical-radio wireless systems has been proven. Resource management in FSO-RF wireless communication systems is a suitable solution to the challenge of increasing data transmission speed. The resources available in optical communication systems include frequency band, memory, and power, with a focus in this proposal on managing optimal PA in real time. On the other hand, there are many analytical solutions for designing optimal power allocation, which, due to the presence of bulky mathematical relations, will require high processing in implementation. Therefore, they cannot be applied to real-time PA[6–10]. However, the innovative use of neural networks, with their appropriate accuracy and speed, can be a game-changer for achieving optimal PA in optical transmission systems. On the other hand, the speed and accuracy of artificial neural networks (ANN) in the inference phase have led to good results in the research, development, and design of cloud infrastructures on which ANNs are trained[10–12]. Although the training phase of ANNs is long, the inference and testing phase provides a good response speed for real-time problems[13]. Therefore, when we want to perform an inference task in real time, using an ANN would be a good choice. Considering the mentioned advantages, researchers have turned to machine learning in recent years to solve the PA problem with high accuracy[14]. Also, various ANN structures have been tested in different wireless scenarios, most of which use a purely data-driven approach and consider the ANN as a black box that is trained on the PA problem for a specific network configuration under one particular condition of the

[1]Faculty of Electrical Engineering, Shahid Rajaee Teacher Training University, Tehran, Iran. [2]Nano-Photonics and Optoelectronics Research Laboratory (NORLab), Shahid Rajaee Teacher Training University, Tehran 16788-15811, Iran. [3]Department of Electrical Engineering, University of Guilan, Guilan, Iran. ✉email: s_olyaee@sru.ac.ir

communication channel. In summary, the authors of[15] suggest that data-driven techniques should not substitute mathematical-driven models, but should complement them.

Salhab et al. conducted a study on a multi-user free-space optical (FSO) and radio frequency (RF) hybrid relay network with opportunistic transmission scheduling[16]. The main results indicate that, under weak atmospheric turbulence conditions, the performance of the system is primarily influenced by the RF channels, which ensure the achievement of diversity order. In contrast, under strong atmospheric turbulence conditions, the system performance is governed by the FSO channel, and the diversity order is determined by the minimum values of turbulence fading and pointing error parameters. In a separate study, Li et al. examined the effectiveness of parallel FSO-RF transmission in satellite-air-ground integrated networks (SAGIN)[17]. They took into account the influence of weather conditions and the quality of service (QoS) for ground users. The numerical results indicated that the energy efficiency of the proposed parallel scheme improved by 30.9% compared to the FSO scheme alone, at a total transmit power of 15 dBW. Alsulami et al. developed a mixed-integer linear programming (MILP) model to optimize resource allocation in wavelength division multiple access (WDMA) optical wireless systems[18]. The study considers two scenarios, each involving 10 users. The results show that all users in both scenarios achieve an optical channel bandwidth exceeding 7.8 GHz. Additionally, the rise of data-driven methods, such as deep neural networks (DNNs), has generated significant interest in modern communication tasks.

The findings in Sun et al.'s research indicate that their proposed approach not only adapts quickly and seamlessly to new scenarios but, more importantly, also sustains high performance in previously encountered scenarios[19]. In a separate study, Alazwary et al. developed and trained a DNN to allocate power for the sender's messages while meeting users' demands[20]. The results indicate that the trained DNN model exhibits good accuracy. Li et al. conducted a study on a MIMO FSO system operating in multiplexing mode[21]. They suggested a PA algorithm that employs a reinforcement learning (RL) method to maximize average capacity over short time intervals. The results indicate that their RL algorithm surpasses the performance of existing benchmarks. In a separate study, Aletri et al. suggested two mixed integer linear programming (MILP) models to conduct a numerical analysis of network and processing in optical wireless (OW) systems[22]. The results indicate that resource allocation in this study was performed optimally. Khadmaoui et al. propose a new framework called G-LiFi 5, which aims to ensure quality of service (QoS) by establishing specific requirements[23]. Their research indicates that employing heterogeneous networks, which combine optical wireless communication (OWC) with radio frequency (RF), is an effective solution for optimizing and harnessing different spectrums. This approach ultimately enhances the QoS experienced by users. Shi et al. proposed a satellite-based wireless sensor network (WSN) that integrates WSNs with cognitive satellite ground networks[24]. This paper presents energy-efficient optimal PA methods for both unrealistic and real-time applications within cognitive satellite ground networks, aiming to maximize the energy efficiency (EE) of the mind satellite user.

Enayati et al. analyzed the PA problem aimed at maximizing the throughput in hybrid communication systems that combine FSO-RF technologies[25]. They examined two schemes: soft switching (SS) and hard switching (HS). Their findings indicate that, for any given visibility level, the spectral efficiency achieved using the soft switching scheme is consistently higher than that obtained with hard switching. In a different study, Ben et al. optimized the PA coefficients and the harvesting term in hybrid FSO-RF communications using non-orthogonal multiple access (NOMA)[26]. The results indicated that by optimizing both the PA and the harvesting duration, the throughput of RF-FSO communications can be significantly increased. Youssef et al. examine the development of a layer two modem that seamlessly integrates both RF and FSO links, ensuring error-free transmission and QoS capabilities[27]. Practical data gathered from a 30 km terrestrial connection shows how the modem works in conjunction with a commercial RF link and offers valuable insights into the system's QoS performance. In another study, Amirabadi et al. introduced a hybrid communication system that combines FSO-RF[28]. Technologies utilize a dual relay. In this system, an access point connects indoor users to the base station through a parallel mixed FSO-RF link. This suggested setup significantly reduces power consumption while maintaining optimal system performance. Bopardikar et al. supply a complete study of hybrid FSO-RF procedures, which integrate FSO-RF communication technologies[29]. This review highlights how these hybrid systems are formed to enable fast and dependable communications, effectively bridging the gap between rate and safety. Li et al.. proposed a hybrid switching scheme that combines FSO and RF for an integrated satellite-air-terrestrial network[30]. This scheme takes into account the effects of weather and leverages legacy channel state information. The numerical results demonstrate that the proposed approach achieves a power outage probability gain of over 8.8 dB and an average BER improvement of more than 8.1 dB.

In a recent study, Adardour et al. aimed to investigate and analyze the performance of a point-to-point optical network using a FSO communication system[31]. They proposed a highly efficient solution to address the challenges faced by FSO links to enhance their reliability, utilizing a beta-mean recursive estimator. Additionally, numerical results were presented to validate their proposal by evaluating the performance of the transmission link in terms of bit error rate and Q factor. Adardour et al. conducted a comprehensive study of a point-to-point optical link system under a Free-Space Optical Communication MIMO channel using an optimized modulation scheme[32]. The results demonstrate a significant improvement in the BER in this research. In another study, Derouiche et al. demonstrated that millimeter waves enable high data rates in FSO communication with significant capacity over short distances[33]. This paper also explores a hybrid FSO/MMW MIMO system that utilizes various modulation techniques under different disturbance conditions. The proposed system is validated by successfully transmitting images while maintaining a suitable constant BER. In a separate study, Hayle et al. demonstrated an innovative high-speed two-way transmission system that combines FSO communication with a 5G wireless link. They utilized a high-power erbium-doped fiber amplifier to compensate for additional losses[34]. The results indicate that this FSO-5G two-way wireless communication system provides a high-speed and cost-effective solution for expanding 5G coverage in both densely and sparsely populated areas.

In this paper, we first generate the necessary data using the Weighted Least Mean Square Error (WMMSE) analytical method for the RF channel, along with the bit error rate (BER) calculation algorithm, as illustrated in Fig. 1. After generating the initial data, we proceed with preprocessing and prioritization of the input data to prepare for neural network training. Once the data is preprocessed, it is applied to the neural models for training. The results obtained on a Windows operating system are then generalized on the Jetson Nano. To do this, we prepare the board and install the required libraries. After ensuring that all software prerequisites are met, we launch the trained network on the hardware. Following this, we receive output from the Embedded PA System, and we perform post-processing and standardization of the neural network output data for evaluation and validation. We then compare these outputs with the results from the analytical methods. Finally, we test the designed models using different data from various configurations of the FSO-RF system, and we evaluate the overall system performance.

Materials and methods

To generate the data needed for training neural models in the Embedded PA System, PA is initially carried out using established analytical methods. For the FSO channel, the BER calculation method is applied across a range of transmitter powers. This approach allows PA to be based on both BER and SNR for the FSO channel. In the case of the RF channel, the WMMSE method serves as the benchmark for optimization and power allocation.

Analytical PA for the FSO channel

In designing the analytical PA technique for the FSO channel, a transmitter power range of 0.1 to 5 mW is considered. BER and SNR values are calculated for different modulation schemes, including Non-Return-to-Zero (NRZ), Return-to-Zero (RZ), Pulse Position Modulation (PPM), and Pulse Width Modulation (PWM), using both Gamma-Gamma and Log-Normal channel models. Additionally, BER and SNR values are examined for various receiver and transmitter aperture diameters, as well as for different deviation angles, to conduct a comprehensive study. For optimal power allocation, higher transmitter power values are assigned to channels with high BER and low SNR. In comparison, lower power values are allocated to channels with low BER and high SNR. To allocate analytical power for BER and SNR, we start by generating random binary bits for the input of the FSO system, as shown in Fig. 1. These random bits are then sampled based on the available memory space, with the number of samples determined during the initial parameter (listed in Table 1) definition phase. Increasing the number of samples enhances the transmitted data rate; however, it also results in a decrease in transmission speed. By understanding the average output light for each modulation type, as well as the power ratio between bit 1 and bit 0, we can calculate the maximum and minimum power values corresponding to bits 0 and 1 for zero and one switching modulation using:

$$\mathbf{P}_1 = \frac{2 \times \mathbf{P_{avg}}}{1 + \frac{1}{\mathbf{M_e}}} \; \mathbf{P}_0 = \frac{2 \times \mathbf{P_{avg}}}{1 + \mathbf{M_e}} \tag{1}$$

According to Eq. (2), the optical signal is produced at the transmitter side by multiplying the generated electrical signal by ΔP and adding the necessary optical power offset to achieve the average optical power.

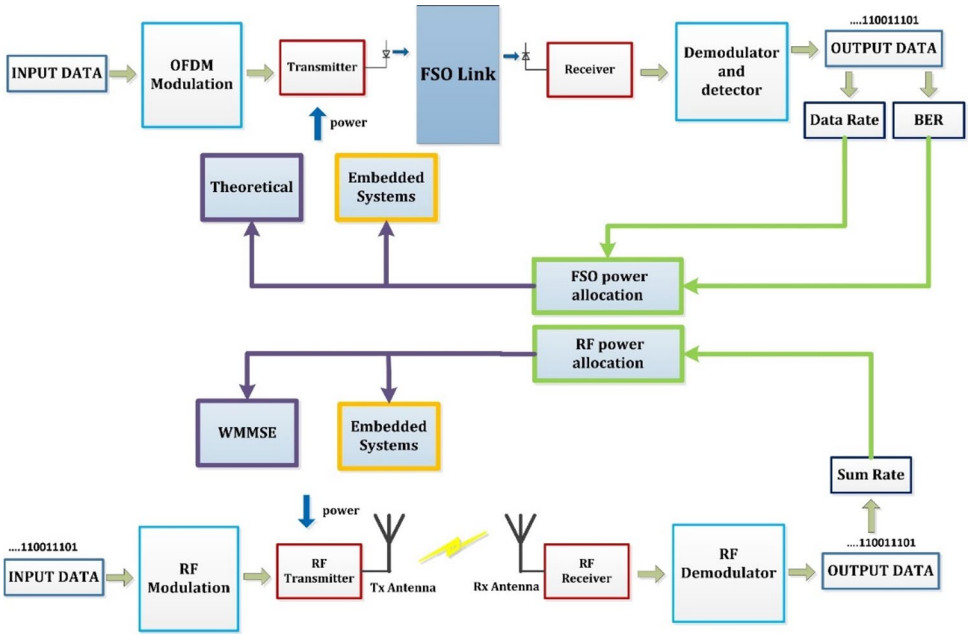

Fig. 1. Comprehensive embedded and analytical PA system for FSO-RF wireless communication channels.

Parameter	Value	Unit
Optical average power - start value	0.1	(mW)
Optical average power - stop value	4.8	(mW)
Optical average power - step value	100	--
Number of bits for each burst transmission	5×10^6	--
Number of samples per bit	5	--
Laser wavelength	1550	(nm)
Laser drive current	5	(mA)
Laser bandwidth	10	(Gbps)
Background light power	0.01	(mW)
Miscellaneous channel loss	0	(dB)
Link Length	500	(m)
Pointing errors, horizontal jitter	0.5	(m)
Receiver aperture diameter	5	(mm)
Responsivity of photodiode	0.5	(A/W)
Transimpedance amplifier gain	10	(V/A)
Noise equivalent power of optical receiver	1×10^{-12}	(W/sqrt(Hz))
Receiver load impedance	50	(Ohms)
Input data format	NRZ, RZ	--
horizontal beam size	5	(mm)
Vertical beam size	5	(mm)
Laser beam divergence angle	10	(Deg)
Electron charge	$1.60217662 \times 10^{-19}$	(C)
Extinction ratio	20	--
Rician factor	10	--
Standard deviation of shadowing	8	(dB)
Cn^2	4×10^{-14}	$m^{-2/3}$
Turbulence strength (α,β)	2,1	--
Fading variance	7	dB

Table 1. The initial parameters[40].

$$P_{opt} = \Delta P \times S_{elec} + P_{avg} \tag{2}$$

At the receiver, the threshold level for extracting the received bits is determined based on the average value of the received electrical signal. Each received bit's midpoint is compared with this threshold to identify whether the received bit is a 0 or 1. For adaptive thresholding, the average length of the entire received signal is divided into smaller segments. Additionally, the BER and SNR values are affected by changes in the diameters of the transmitter and receiver apertures, as well as the deviation of the transmitted protocol. The beam radius at the receiver is calculated using Eq. (3)[35,36], where $\boldsymbol{w}_0$, L, and $\boldsymbol{\lambda}_0$ represent the aperture radius, link length, and source wavelength, respectively.

$$\mathbf{W}_{\mathbf{R_x}} = \boldsymbol{w}_0 \times \sqrt{1 + \left(\frac{\boldsymbol{L}}{\boldsymbol{\pi} \times \frac{\boldsymbol{w}_0^2}{\boldsymbol{\lambda}_0}} \right)^2} \tag{3}$$

The ratio of the aperture size to the vertical beam size is defined by Eq. (4)[35,36]. In this equation, $\mathbf{R}_{\mathbf{x-Ap_{dia}}}$ represents the diameter of the receiver aperture, while $\mathbf{W}_{\mathbf{R_{x-v}}}$ denotes the radius of the vertical beam within the receiver.

$$\mathbf{V}_{\mathbf{PE_v}} = \sqrt{\frac{\boldsymbol{\pi}}{2}} \times \frac{\mathbf{R}_{\mathbf{x-Ap_{dia}}}}{2 \times \mathbf{W}_{\mathbf{R_{x-v}}}} \tag{4}$$

Equation (5)[35,36] determines the equal vertical beam size at the receiver. In this equation, the error function, $\mathbf{erf}\,(\mathbf{V}_{\mathbf{PE_v}})$, represents the ratio of the aperture size to the vertical beam size. This procedure is determined based on the radius of the vertical beam at the receiver and the ratio of the aperture size to that vertical beam.

$$\mathbf{W}_{2-\mathbf{eq}-\mathbf{PE}_\mathbf{v}} = \frac{\mathbf{W}^2_{\mathbf{R}_{\mathbf{x}-\mathbf{v}}\sqrt{\pi}\,\mathbf{erf}\left(\mathbf{V}_{\mathbf{PE}_\mathbf{v}}\right)}}{2\mathbf{V}_{\mathbf{PE}_\mathbf{v}}\mathbf{exp}\left(-\mathbf{V}^2_{\mathbf{PE}_\mathbf{v}}\right)} \tag{5}$$

The proportion of the aperture size to the horizontal beam and the equivalent horizontal beam size on the receiver side is defined as follows[35,36]:

$$\mathbf{V}_{\mathbf{PE}_\mathbf{h}} = \sqrt{\frac{\boldsymbol{\pi}}{2}} \times \frac{\mathbf{R}_{\mathbf{x}-\mathbf{A}_{\mathbf{pdia}}}}{2 \times \mathbf{W}_{\mathbf{R}_{\mathbf{x}-\mathbf{v}}}} \tag{6}$$

$$\mathbf{W}_{2-\mathbf{eq}-\mathbf{PE}_\mathbf{h}} = \frac{\mathbf{W}^2_{\mathbf{R}_{\mathbf{x}-\mathbf{h}}\sqrt{\pi}\,\mathbf{erf}\left(\mathbf{V}_{\mathbf{PE}_\mathbf{h}}\right)}}{2\mathbf{V}_{\mathbf{PE}_\mathbf{h}}\mathbf{exp}\left(-\mathbf{V}^2_{\mathbf{PE}_\mathbf{h}}\right)} \tag{7}$$

In the context of a noisy channel, the BER is calculated using Eq. (8)[37,38], which is derived from the log-normal distribution model based on the Gauss-Hermite quadratic Eqs[37,38]. Additionally, $\mathbf{I}_0\,(0)$indicates the adjusted zero-order Bessel function of the first kind.

$$\mathbf{BER} = \frac{1}{\boldsymbol{\pi}} \sum\nolimits_{\mathbf{i}=1}^{\mathbf{k}} \boldsymbol{\omega}_{\mathbf{i}} \mathbf{Q}\left[\frac{\boldsymbol{\eta}\,\mathbf{I}_0}{\sqrt{2\mathbf{N}_0}}\,\mathbf{exp}\left(-2\boldsymbol{\sigma}^{\,2}_{\mathbf{x}} + \mathbf{x}_\mathbf{i}\sqrt{9\boldsymbol{\sigma}^{\,2}_{\mathbf{x}}}\right)\right] \tag{8}$$

In the Gamma-Gamma distribution model, the BER values are derived from Eq. (9)[37,38].

$$\mathbf{BER} = \frac{2^{\alpha+\beta-3}}{\sqrt{\pi^3\,(\alpha)\,(\beta)}}\mathbf{G}^{2,4}_{5,2}\left[\left(\frac{2}{\alpha\beta}\right)^2 \times 2 \times \frac{\eta\mathbf{I}_0}{\sqrt{2\mathbf{N}_0}} \;\middle|\; \begin{matrix} \frac{1-\alpha}{2}, & \frac{2-\alpha}{2}, & \frac{1-\beta}{2}, & \frac{2-\beta}{2}, 1 \\ 0, & \frac{1}{2} & & & \end{matrix}\right] \tag{9}$$

Where $G^{2,4}_{5,2}\,[0]$ is the Meijer G function, the BER values with chaotic channel conditions and pointing error are calculated from Eq. (10)[32,39,40] with the Gamma-Gamma distribution model. This equation is approximated for high values of SNR.

$$\mathbf{BER} = \frac{2^{\beta-1}\left(\frac{\alpha}{2}+\frac{1}{2}\right)\mathbf{exp}\left(\frac{\mathbf{s}^2}{2\sigma_\mathbf{s}^2} + \frac{-\mathbf{s}^2\gamma^2}{2\beta-2\gamma^2}\right)\left(\frac{\alpha\beta}{\mathbf{A}_0}\right)^\beta}{(\alpha)\;(\beta)\sin\left[(\alpha-\beta)\,\pi\right]\;(-(\alpha-\beta)+1)\,|\gamma^2-\beta|\,\beta} \times \left(\frac{\beta+1}{2}\right)\sqrt{\pi}\gamma^2\left(\frac{\eta\mathbf{I}_0}{\sqrt{2\mathbf{N}_0}}\right)^{-\frac{\beta}{2}} \tag{10}$$

Data rate values are determined using Eq. (11) based on the number of samples per bit, bandwidth, and signal-to-noise-and-interference ratio.

$$Data\ Rate = \mathrm{Nos} \times\ B \times \log_2\left(1 + \mathrm{SINR_k}\right) \tag{11}$$

Analytical PA for the RF channel

For the RF channel, the WMMSE method is utilized for analytical power allocation. WMMSE, which stands for Weighted Minimum Mean Square Error, is an optimization-based approach designed to allocate power in wireless networks. Its main objective is to minimize the mean square error (MSE) between the desired signal and the actual received signal. Additionally, this method accounts for interference from other users and background noise, making it an effective strategy for mitigating multi-user interference.

The channel coefficients for each user can be modelled using Rayleigh, Rician, log-normal, or gamma fading. For simplicity, we assume that all users are subjected to a random fading channel model. The objective is to allocate power P_k to each user while ensuring that the aggregate transmitted power does not transcend a specified maximum power limit. The received signal for the k-th user is defined as follows: the first part, Equation (12)[41] represents the desired transmitted signal, while the second part accounts for interference. In this context, denotes the channel coefficient from the transmitter to the k-th user. Additionally, S_j and S_k denote the data symbols for the j-th and k-th users, while n_k signifies the white Gaussian noise.

$$y_k = h_k^H v_k s_k + \sum\nolimits_{j \neq k} h_k^H v_j s_j + n_k \tag{12}$$

The signal-to-interference plus noise ratio for the k-th user is defined by Eq. (13)[41]. In this equation, $\boldsymbol{p_k}$ represents the power allocated to the k-th user, $|\boldsymbol{h_k}|^2$ denotes the channel gain, $\boldsymbol{\sigma}^2$ indicates the noise power, and $\boldsymbol{p_i}$ is the power allocated to other users.

$$\mathrm{SINR_k} = \frac{\mathrm{p_k}|\mathrm{h_k}|^2}{\sum_{\mathrm{i}\neq\mathrm{k}}\mathrm{p_i}|\mathrm{h_i}|^2 + \sigma^2} \tag{13}$$

The objective of WMMSE is to minimize the mean square error (MSE) between the received signal and the desired signal. The primary aim is to reduce the weighted MSE for all users while taking interference into account. The PA based on WMMSE for a downlink wireless communication system can be expressed as Eq. (14)[41]. By

adjusting the power allocation, the total MSE for all users is minimized. In this equation, $\boldsymbol{y_k}$ represents the received signal, while $\widehat{\boldsymbol{y}}_{\boldsymbol{k}}$ denotes the estimated signal for the k-th user.

$$(\mathrm{p}) = \sum {}_{k=1}^{K}\mathbb{E}\left[|y_k - \widehat{y}_k|^2\right] \tag{14}$$

In Rician fading, the channel consists of a dominant line-of-sight (LoS) component along with additional scattered (non-line-of-sight) components. The Rician fading model is defined by the coefficient K, which indicates the ratio of the power of the LoS component to the power of the scattered components. The channel coefficient $\boldsymbol{h_k}$ for user k is defined by the Rician fading model as shown in Eq. (15)[41].

$$\mathrm{h_k} = \sqrt{\frac{\mathrm{K}}{\mathrm{K}+1}}\mathrm{H_{LOS}} + \sqrt{\frac{1}{\mathrm{K}+1}}\mathrm{H_{NLOS}} \tag{15}$$

The Rician coefficient K controls the ratio of line-of-sight signals to scattered signals. A higher value of K indicates a stronger line-of-sight component compared to scattered signals. The gamma distribution is commonly used to model mixed fading, which encompasses multipath fading and shadowing, particularly when dispersion is dominant. According to Eq. (16)[41] in this model, the channel power gain $|\boldsymbol{h_k}|^2$ is represented as a random variable that follows a gamma distribution.

$$|h_k|^2 = Gamma(\alpha,\theta)(\alpha,\theta > 0) \tag{16}$$

Rayleigh fading is a phenomenon encountered in wireless communications. It is a statistical model that describes how the propagation environment affects a radio signal, such as the signals used by wireless devices. This model is particularly relevant when there is no dominant line-of-sight component between the transmitter and receiver, resulting in the signal being scattered across multiple paths. The channel coefficient in Rayleigh fading can be expressed as Eq. (17)[41]: $\boldsymbol{a_k}$ represents the amplitude of the Rayleigh distribution, while $\varnothing_{\boldsymbol{k}}$ denotes the phase of the uniform distribution.

$$h_k = a_k e^{j\varnothing_k} \tag{17}$$

In wireless communications, log-normal shadowing models large-scale path loss due to shadowing caused by obstacles (e.g., buildings, terrain). The channel coefficient in this model is defined as in Eq. (18)[41].

$$PL\,(d) = PL\,(d_0) + 10n\log_{10}\left(\frac{d}{d_0}\right) + X_\sigma \tag{18}$$

$$|h_k|^2 = 10^{-\frac{PL(d)}{10}} \tag{19}$$

The optimization problem is addressed iteratively by allocating transmit powers, denoted as $\boldsymbol{p_k}$, to each user while minimizing the total mean square error (MSE). The power allocated to each user k in the WMMSE approach is updated in each iteration according to the MMSE and Signal-to-Interference-plus-Noise Ratio (SINR) filters. Equation (20)[42] illustrates the update process for power allocation.

$$\mathbf{p_k} = \frac{|\mathbf{h_k}|^2}{\sum_{\mathbf{i}\neq\mathbf{k}}|\mathbf{h_i}|^2 + \boldsymbol{\sigma}^2} \times \mathbf{SNR_{lin}} \tag{20}$$

According to Eq. (21), the total power allocated to all users must not exceed the maximum power limit. This process iterates until the PA converges to a solution that minimizes the MSE.

$$\sum {}_{k=1}^{K}\boldsymbol{p_k} \leq \boldsymbol{P_{max}} \tag{21}$$

Also, the corresponding sum rate for each user is calculated using the Shannon capacity formula, which is shown in Eq. (22)[43].

$$\mathbf{Sum\ Rate} = \sum {}_{\mathbf{k}=1}^{\mathbf{K}}\mathbf{B}\log_2(1+\mathbf{SINR_k}) \tag{22}$$

Embedded PA system design for FSO-RF channel

This paper introduces a novel approach to designing an algorithm for power allocation for a hybrid FSO-RF system, which specifically addresses the problem of real-time optimal power allocation. This algorithm offers significant optimizations in accuracy and processing time, which are significantly improved compared to the methods in the introduction. This paper is also more comprehensive than other works, including a broader range of wireless communication channels under various conditions, as detailed in the results section.

Jetson Nano is another key innovation of the paper, utilizing this platform to implement deep learning algorithms. In this innovation, the open-source nature of the project enables direct deployment without computer intermediaries in wireless communication systems, facilitating optimal management. We specifically address the

power management challenges by implementing neural models on suitable hardware and demonstrate that these neural models can perform well under various wireless communication channel conditions.

Another unique feature of this paper is the detailed analysis of the accuracy-delay tradeoff, which is important for use in embedded systems with real-time constraints due to the varying conditions of optical-radio wireless channels. In this paper, we show how these two criteria can be effectively managed to arrive at an optimal model for real-time optimal power allocation.

In this section, we propose the design and implementation of a PA optimization problem in optical-radio wireless systems. This study utilizes neural networks to improve the precision and comprehensiveness of the PA system for these communication systems. The design of the neural network and the generation of training data were specifically tailored to achieve this goal. Consequently, the introductory purpose of the research is to maintain acceptable performance across various values of wireless network parameters. Additionally, certain conditions were identified for optimizing PA in optical-radio communication systems. The first requirement is the system's accuracy, which means that the total data transmission rate achieved by the proposed method should be comparable to near-optimal benchmark algorithms, such as WMMSE and the BER calculation algorithm for the input power.

The second requirement focuses on dynamics and simplicity, emphasizing minimal mathematical calculations. This method allows the optimization problem to be solved in real time while using minimal computational resources, resulting in faster processing speeds. The third requirement is ensuring compatibility and scalability with various wireless networks. The optimization problem involves several dynamic parameters, including the number of users. The proposed method enhances performance reliability by adjusting various wireless configuration parameters and can be easily implemented using a DNN architecture. The training data generated from benchmark algorithms are preprocessed and normalized to enhance processing speed before training the neural model, thus improving overall system efficiency.

After training the neural models, they are deployed on the Jetson Nano platform. The output of the embedded PA system is then compared to the analytical PA results for validation. The optimal power allocation, as illustrated in Fig. 2, regulates the power of the optical-radio wireless communication channel. In summary, this system processes the data transmission rate and the total rate for both the optical and radio channels across various channel conditions and types of transmitters and receivers. It then performs real-time optimal PA for each channel using two three-layer DNNs.

The neural model was designed using the TensorFlow framework and employs a Fully Connected Feed-forward Neural Network, also known as a Multilayer Perceptron. In this paper, neural models are trained with diverse data. The number of training data points in the RF channel is 13,000, and the number of test data points is 2,500. Also, the number of training data in the FSO channel is about 40,000, and the number of test data is 6,500.

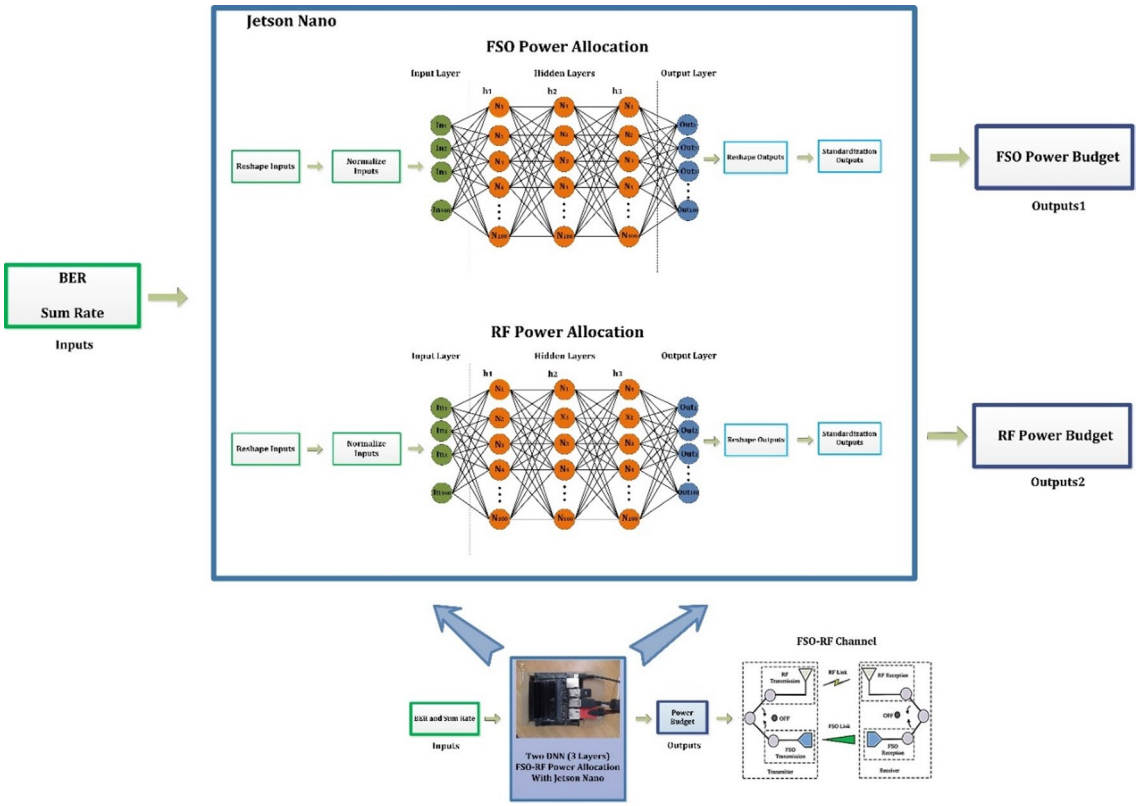

Fig. 2. Structure of the embedded PA system.

An initial hyper parameter search was also performed to investigate the effects of the number of layers and neurons. In this process, different values of the number of layers and neurons (including values of 50 to 200 neurons per layer) were tested. The results showed that several 100 neurons per layer effectively maintained the accuracy of the model while significantly reducing the processing time. Choosing the number of layers and neurons at this size was especially important to maintain the simplicity of the model and avoid overfitting.

To ensure the generalization of the DNN model in different scenarios, our training data includes various fading conditions and correlated channels. We have used different fading distributions, such as Rayleigh, Rician, and Nakagami, so that the model can simulate different channel conditions. Also, the data are selected to cover the diversity of channel conditions, so that the model can perform well in new scenarios in general. The data was reshaped and normalized to enhance the model's processing speed and accuracy. After preprocessing the training data, a DNN with three layers, each containing 100 nodes, was trained. The model uses the ReLU activation function, the Adam optimization algorithm, and the MSE cost function. The training configurations included a batch size of 100, a learning rate of 0.001, and a total of 1,200 training steps. After training the DNNs, we apply the preprocessed inputs and the test dataset to derive the predicted power allocations.

The three-layer architecture with 100 neurons per layer is known as a basic model for most deep learning problems in the field of resource allocation and similar problems in communication networks. This number of neurons is suitable for modeling the complexities of FSO and RF channels, as well as the balance between accuracy and processing time. The number of neurons in each layer has been selected in a way that ensures high model scalability without compromising the efficiency and processing speed, based on experimental analyses and the study of different models. Also, preliminary studies have shown that a three-layer architecture with 100 neurons per layer is effectively able to learn complex features and nonlinear dependencies in FSO and RF channel data. In our experiments, increasing the number of neurons per layer resulted in increased complexity and computational time, without significantly increasing the accuracy of the model. For this reason, choosing 100 neurons per layer provides a good balance between accuracy and processing speed.

On the other hand, generalization analysis was performed in comparison with classical methods to prove the generalization ability of the DNN model, compared to analytical power allocation methods such as WMMSE and other algorithms. The results show that DNN performs well with test data in scenarios where channel conditions change and, considering different scenarios for the wireless channel, can have better generalization than these other machine learning methods. Considering the complexity and large number of calculations involved in the wireless channel scenario with mobile users, this scenario is proposed for future research at the end of the conclusion. With this approach, our model has performed effectively in uncertain conditions and new scenarios, and we have shown that the generalization ability of the model is well preserved.

The neural models are implemented on the Jetson Nano to compare and validate their outputs against benchmark PA algorithms. In the context of wireless radio system power allocation, we compare the sum rate obtained from executing the WMMSE algorithm with the results generated by the trained DNN. For optical channel power allocation, we also compare the analytical values derived from the BER calculation algorithm with the outputs of the embedded PA system designed for the optical wireless channel.

The choice of a dual-DNN architecture with parallel processing for the FSO and RF channels has technical and practical reasons. The first reason is the different nature of the FSO and RF channels, which have different statistical, noise, and attenuation characteristics. The FSO channel is susceptible to atmospheric conditions such as fog and rain, while the RF is affected by fading and electromagnetic interference. Using a single network would have prevented the model from learning and managing these inherent differences well. Designing two separate networks allows the model to manage power allocation based on the specific characteristics of each channel.

The second reason is the increased accuracy in independent processing, which, by processing the FSO and RF channel data in parallel, each network can better train its own channel-specific structures and patterns. Our experiments and the graphs in the article reveal that the transmitter power budget ranges for the two FSO and RF channels differ significantly.

Also, using two parallel models at the final decision-making level is a great advantage over a unified architecture that must learn from the beginning how to manage information from both channels simultaneously and correctly, which in practice increases the complexity of training and causes overfitting on limited data.

The use case may require a higher quality of service, which means that the priority for allocating these communications can be greater than that for other applications. To allocate more power to receivers with higher priority, a weight α_k (ranging from 0 to 1) is applied to the PA matrix. These weights provide the system with enhanced control over the DNNs by using them to the parameters of each communication channel.

Results

PA is a significant and challenging real-time optimization problem in managing optical-radio wireless networks. Traditional analytical PA methods involve complex mathematical calculations and can be time-consuming. To address these issues, this paper proposes the use of deep learning to develop a real-time PA system that reduces processing time while maintaining accuracy. In this approach, two DNNs are trained separately on a Jetson Nano to handle PA for each optical-radio wireless channel in parallel.

In the radio communication channel, PA has been performed using Gamma-Gamma and Log-Normal distribution models, along with Rayleigh and Rician fading. The implemented real-time optimal PA for 10, 20, and 30 users has been compared and validated against the WMMSE benchmark method. Additionally, for the wireless optical communication channel, PA has been conducted using Log-Normal and Gamma-Gamma distribution models, also incorporating Rayleigh and Rician fading across various modulation schemes and input shapes. The results of this work have been compared with analytical methods.

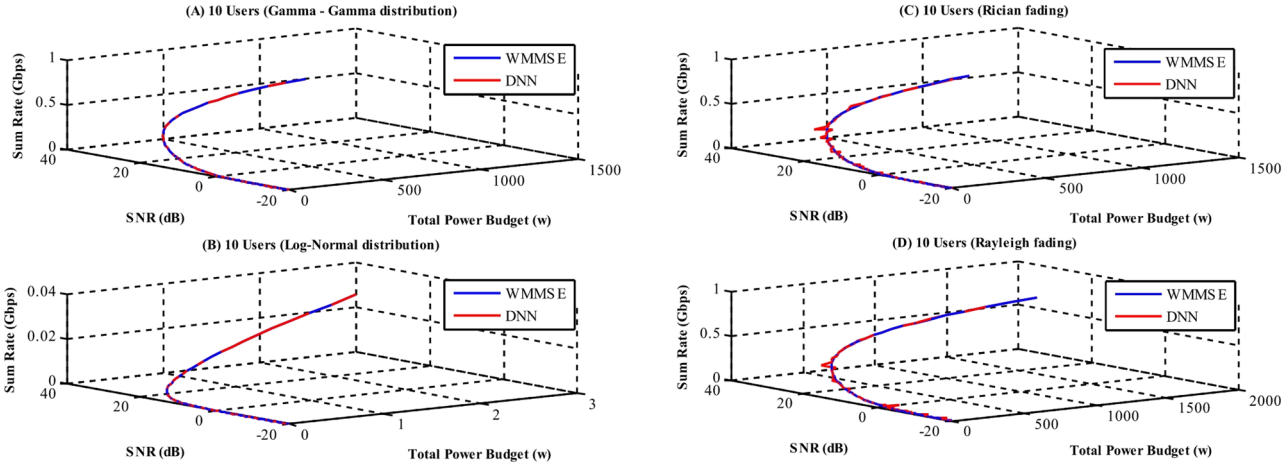

Fig. 3. Sum rate concerning SNR for power budgets in WMMSE and Embedded power allocation methods for 10 users in the RF channel.

Channel type	Min Total Power (W)	Max Total Power (kW)	Min Sum Rate (Mbps)	Max Sum Rate (Gbps)	Accuracy %
Gamma-Gamma	0.1012	1.0331	0.1672	0.6343	99.95
Log-Normal	0.0000151	0.0026	0.0042	0.0030	99.92
Rician fading	0.0117	1.0421	0.1684	0.6534	97.09
Rayleigh fading	0.0309	1.8651	0.301	0.6862	97.03

Table 2. Maximum and minimum sum rates and accuracy values in the embedded PA system for various RF communication channels with 10 users.

Embedded PA to RF channel

In this section, we perform PA for the wireless radio channel using the output from the DNN implemented on the Jetson Nano. The results are compared with those obtained using the benchmark method, WMMSE. Figure 3 illustrates the sum rate values in relation to the SNR for the total power budget in both methods: WMMSE and embedded power allocation, with a total of 10 users. According to Fig. 3; Table 2, the highest total rates observed are as follows: the Gamma-Gamma model shows a rate of 0.6543 Gbps, the Log-Normal model has a rate of 3 Mbps, the Rician fading channel reaches 0.6534 Gbps, and the Rayleigh fading channel records the highest at 0.6862 Gbps. Additionally, the average accuracy of the embedded PA system for the RF channel with 10 users is 98.49%.

In an RF communication channel with 20 users, the accuracy of the embedded PA system decreases by 1% compared to the scenario with 10 users. Figure 4 illustrates the changes in total rate concerning embedded PA and SNR for 20 users in comparison to the WMMSE algorithm. According to Table 3, the average accuracy of the PA system in the 20-user case is 97.91%.

The maximum data transmission rates in various models are as follows: for the Gamma-Gamma distribution model, it is 1.0637 Gbps; for the Log-Normal model, it is 0.1792 Mbps; for the Rician fading channel, it is 1.0551 Gbps; and for the Rayleigh fading channel, it is 0.9494 Gbps. In this case, the data transmission rate increases when compared to the 10-user scenario.

As the number of users increases to 30, the accuracy of the embedded PA system for the RF channel is 0.97. As a result, the total channel rate for the users increases. Figure 5 shows the modifications in total rate based on embedded PA and SNR for 30 users, considering different distribution models and channel fading scenarios.

Table 4 presents the maximum and minimum values for both the total rate and accuracy in the embedded PA system across various RF communication channels with 30 users. According to Table 4, the maximum data transmission rates are as follows: in the Gamma-Gamma distribution model, it reaches 1.4216 Gbps; in the Log-Normal model, it is 0.2588 Mbps; for the channel with Rician fading, the rate is 1.3939 Gbps, while for the channel with Rayleigh fading, it is 0.2814 Gbps.

Some users require a higher quality of service and should therefore be given higher priority in the PA system. In an optimal PA system for RF wireless communication channels, a weighting factor, denoted as α_k, is applied to the PA matrix; this factor ranges from 0 to 1.

Figure 6 illustrates two scenarios: the analytical PA system that does not consider channel priority and the embedded PA system that does. In this example, which includes a channel with 10 users, users 9 and 10 have the highest priority for power allocation, while users 1 and 2 have the lowest priority.

To more practically investigate the performance of the proposed system in real scenarios, evaluations were conducted based on system-level metrics. These evaluations included BER, Throughput, and Outage Probability

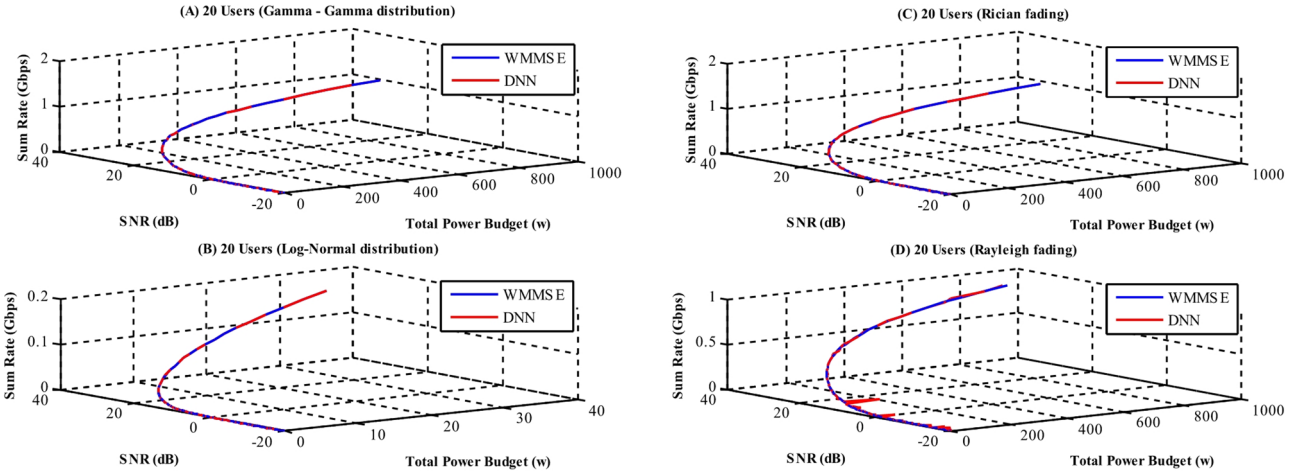

Fig. 4. Sum rate in terms of SNR for total power budget values in the two methods, WMMSE and Embedded power allocation, for 20 users in the RF channel.

Channel type	Min Total Power (W)	Max Total Power (kW)	Min Sum Rate (Mbps)	Max Sum Rate (Gbps)	Accuracy %
Gamma-Gamma	0.0109	0.9585	0.1551	1.0637	99.94
Log-Normal	0.00034	0.0310	0.0052	0.1792	99.92
Rician fading	0.0107	0.9443	0.1526	1.0551	99.89
Rayleigh fading	0.0095	0.8136	0.1344	0.9494	92.03

Table 3. Maximum and minimum values of the sum rate and accuracy in the embedded PA system for various RF communication channels involving 20 users.

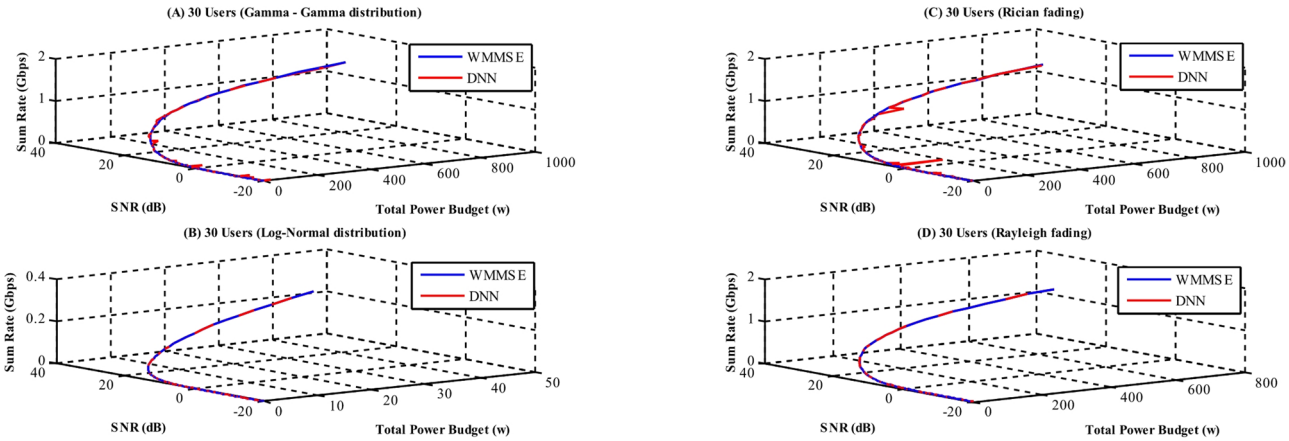

Fig. 5. Sum rate values in terms of SNR for total power budget using two methods: WMMSE and Embedded power allocation for 30 users in the RF channel.

Channel type	Min Total Power (W)	Max Total Power (kW)	Min Sum Rate (Mbps)	Max Sum Rate (Gbps)	Accuracy %
Gamma-Gamma	0.0105	0.9333	0.1510	1.4216	93.65
Log-Normal	0.000458	0.0408	0.0066	0.2588	99.72
Rician fading	0.0100	0.8861	0.1441	1.3939	95.09
Rayleigh fading	0.0083	0.7434	0.1203	1.2814	99.81

Table 4. Maximum and minimum values of the sum rate and accuracy in the embedded PA system for various RF communication channels with 30 users.

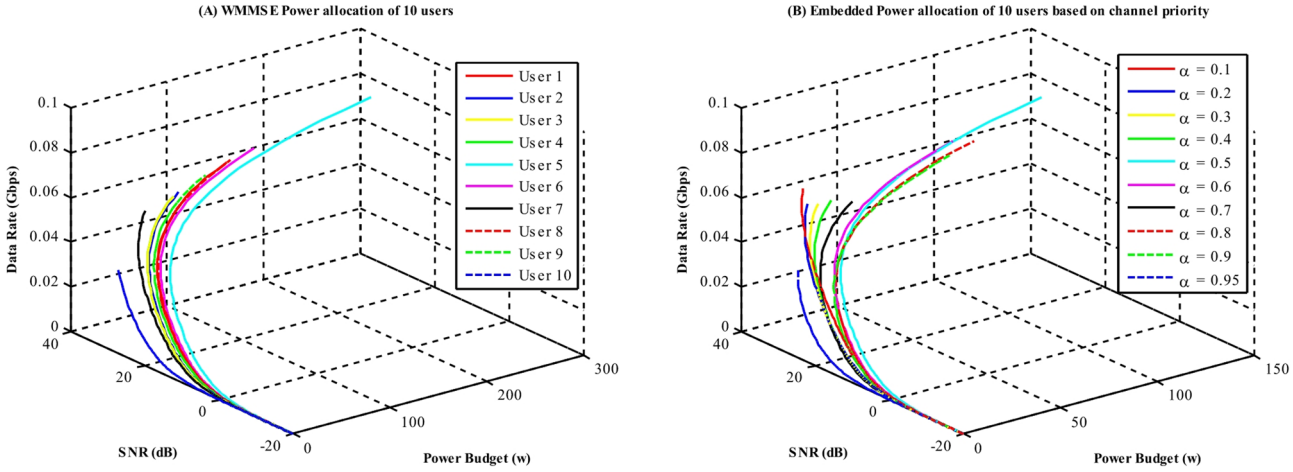

Fig. 6. Analytical power allocation system without channel priority and embedded power allocation system with channel priority coefficients applied in the RF power allocation system.

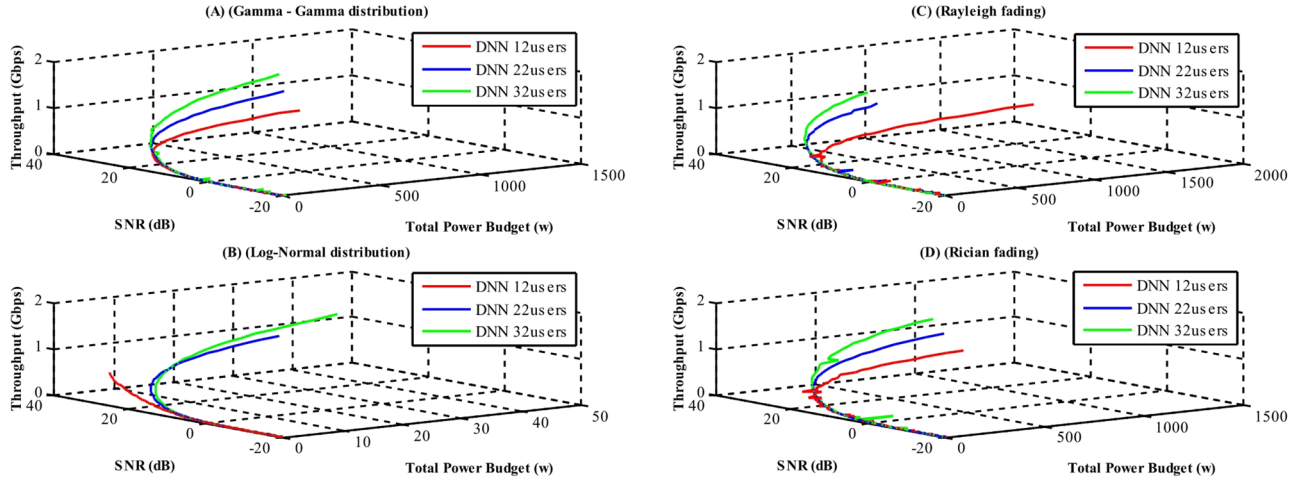

Fig. 7. Throughput variations based on power budget and SNR for the implemented DNN model for different distribution model using the Gamma-Gamma distribution.

Channel type	Min Total Power (W)	Max Total Power (kW)	Min Throughput (Mbps)	Max Throughput (Gbps)
Gamma-Gamma	0.0114	0.9743	0.1505	1.4487
Log-Normal	0.000471	0.0476	0.1543	1.3427
Rician fading	0.0104	0.9241	0.1505	1.4156
Rayleigh fading	0.0091	0.7812	0.1546	1.2464

Table 5. Maximum and minimum values of the throughput in the embedded PA system for various RF communication channels with 32 users.

under varying channel conditions. The results showed that the embedded power allocation system performs close to the WMMSE algorithm in most cases, while imposing much less computational complexity on the system. Figure 7 shows the variations of Throughput in terms of SNR and total power budget in the embedded PA system for 12, 22, and 32 users in the RF channel with the Gamma-Gamma distribution model. Also, the maximum and minimum values of the Throughput values for the Gamma-Gamma, Log-Normal, Rayleigh, and Rician fading distribution models are specified in Table 5.

Figure 8 illustrates the variation of outage probability in relation to SNR for 12, 22, and 32 users within the embedded PA system, based on the Gamma-Gamma distribution model. As shown in Fig. 8, for SNR values exceeding 9 dB, the outage probability remains below 5%.

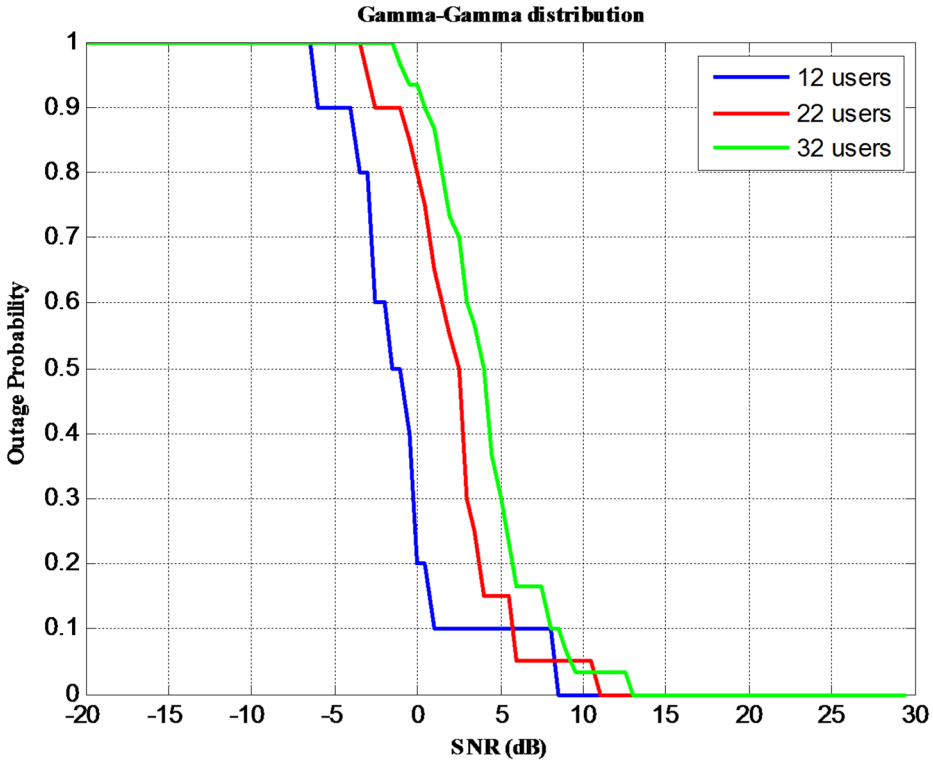

Fig. 8. Outage probability variations based on SNR for the implemented DNN model for 12, 22 and 32 users using the Gamma-Gamma distribution.

Number of users	WMMSE Processing time (s)	DNN Processing time	Processing speed ratio
10	8.949	0.168	53.2
20	35.251	0.156	225
30	64.502	0.171	376.2

Table 6. Processing time in the analytical and embedded PA system with a single-layer DNN for a communication channel with a different number of users.

Also, the results show that using the embedded PA system is more cost-effective as the number of users increases. This latency value should be implemented with more powerful versions of Jetson Nano for many resource allocation and scheduling applications in 5G and even 6G networks that require sub-millisecond scheduling. However, in future research, solutions to improve the processing time will be explored, including the use of more compact models and hardware optimizations using graphics cards or parallel processing extenders to reduce latency.

Processing time is a crucial parameter in designing a real-time optimal power allocation system for the FSO-RF channel. The embedded PA system is designed using single-layer, double-layer and triple-layer DNNs to investigate their processing speed. At the beginning of the neural model design, a single-layer neural network is used to allocate power to the radio communication channel. Table 6 shows the performance comparison of the single-layer neural network and the benchmark analytical algorithm in processing speed for 10, 20 and 30 users. In the outputs in this section, it is observed that the response speed of the neural model is 53 times that of the benchmark power allocation algorithm.

Increasing the number of hidden layers in the DNN to two does not lead to a significant change in processing time. Table 7 presents the processing times for both the analytical and embedded PA systems using a two-layer DNN, along with the ratio of their processing speeds.

The processing time in DNN increases by about 0.004 s with the increasing number of hidden layers. Table 8 shows the ratio of processing speed for the analytical and embedded power allocation systems. According to the results of time analysis, in the RF channel with an increasing number of users, using the embedded power allocation system results in better time saving.

Embedded PA to FSO channel

In designing the Embedded Optimal PA System, PA is initially determined using an analytical method that calculates BER and SNR. This method considers a range of transmitter power from 0.01 to 4.8 mW. High

Number of users	WMMSE Processing time (s)	DNN Processing time (s)	Processing speed ratio
10	8.865	0.166	70.51
20	30.884	0.125	247.1
30	54.108	0.172	318.9

Table 7. Processing time in the analytical and embedded PA system with a two-layer DNN for a communication channel with different numbers of users.

Number of users	WMMSE Processing time (s)	DNN Processing time (s)	Processing speed ratio
10	9.461	0.174	52.8
20	32.678	0.128	255.1
30	46.095	0.156	410.2

Table 8. Processing time in the analytical and embedded power allocation system with a three-layer DNN for a communication channel with different numbers of users.

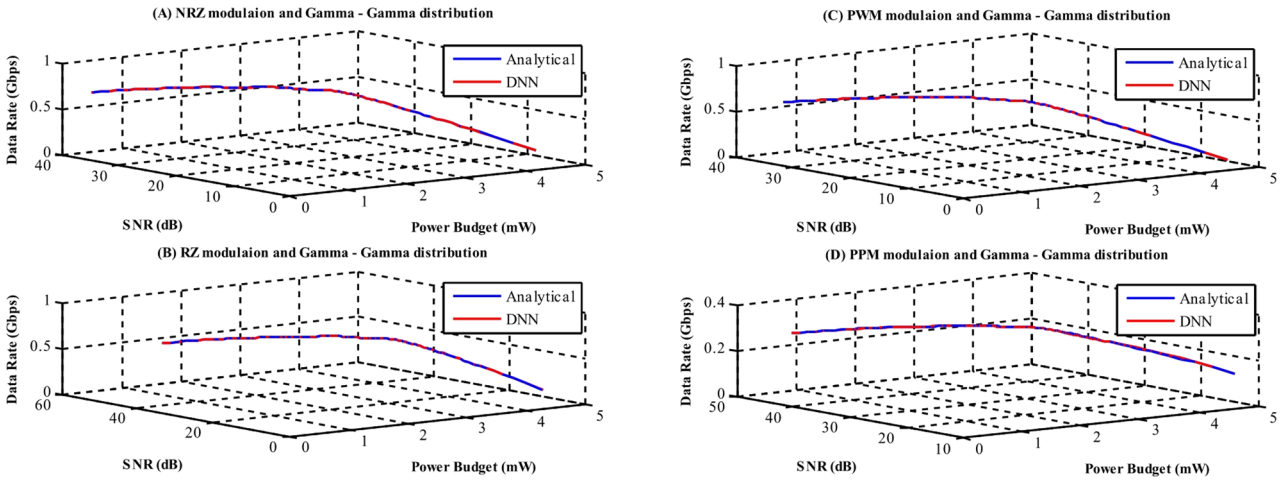

Fig. 9. Data rate variations based on power budget from two analytical methods and the output of the implemented DNN model for different modulations using the Gamma-Gamma distribution.

Modulation type	Min Total Power (mW)	Max Total Power (mW)	Min Data Rate (Gbps)	Max Data Rate (Gbps)	Accuracy %
NRZ	0.4509	4.70	0.1110	0.6580	99.85
RZ	0.4531	4.73	0.1278	0.6787	99.72
PWM	0.4552	4.71	0.0741	0.6065	99.81
4-PPM	0.4554	4.74	0.1466	0.2873	97.81

Table 9. Data rate and accuracy values in the embedded PA system for various modulations in a wireless optical communication channel are analyzed using a Gamma-Gamma distribution model.

transmitter power values are assigned to channels with high BER and low SNR, while low transmitter power values are allocated to channels with low BER and high SNR. Figure 9 illustrates the variations in data rate per power budget derived from the two analytical methods and the output of the implemented DNN model for different modulation schemes and the Gamma-Gamma distribution model. As presented in Table 9, the highest data transmission rates achieved in the Embedded PA System for the wireless optical communication channel using the Gamma-Gamma distribution model are as follows: 0.6580 Gbps for NRZ modulation, 0.6787 Mbps for RZ modulation, 0.6065 Gbps for PWM, and 0.2873 Gbps for 4-PPM modulation.

In the embedded PA for optical wireless communication channels using the Log-Normal model, the accuracy of the DNN is lower compared to that using the Gamma-Gamma model. Specifically, the accuracy of the embedded PA system is 97.71%.

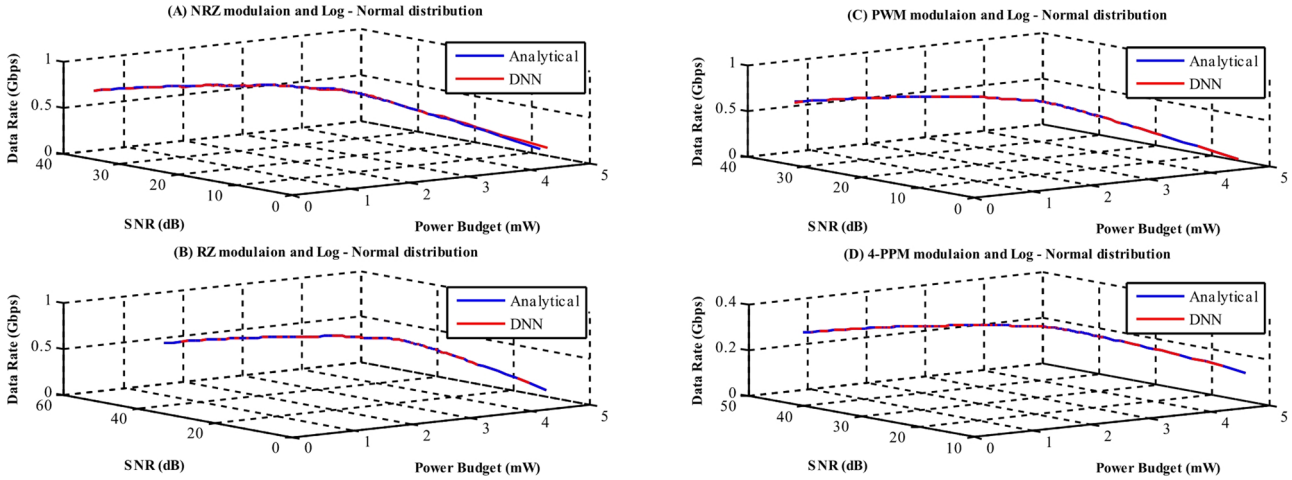

Fig. 10. Data rates and accuracy values in the Embedded Power Allocation System are analyzed concerning SNR for various modulation types in the wireless optical communication channel, utilizing the Log-Normal distribution model through two analytical methods.

Modulation type	Min Total Power (mW)	Max Total Power (mW)	Min Data Rate (Gbps)	Max Data Rate (Gbps)	Accuracy %
NRZ	0.4556	4.81	0.1110	0.6580	92.65
RZ	0.4551	4.72	0.1278	0.6787	99.63
PWM	0.4526	4.71	0.0741	0.2873	99.89
4-PPM	0.4530	4.73	0.1466	0.2814	98.67

Table 10. Maximum and minimum data rates, along with accuracy values, in the embedded PA system for different modulation types within the wireless optical communication channel follow a Log-Normal distribution model.

Figure 10 illustrates the affinity between data rates and accuracy in the embedded PA system as a function of SNR for various modulation types within the wireless optical communication channel using the Log-Normal distribution model. This is analyzed through two analytical methods and the DNN model.

According to Table 10, the highest data rates achieved in the embedded PA system for the wireless optical communication channel with the Gamma-Gamma distribution model are as follows: 0.6580 Gbps for NRZ modulation, 0.6787 Gbps for RZ modulation, 0.2873 Gbps for PWM modulation, and 1.2814 Gbps for 4-PPM modulation.

In the FSO channel, two critical factors in the design of the PA system are the beam deflection angle and the diameter of the transmitter aperture. Figure 11 shows the changes in the data transmission rate within the embedded PA system. It analyzes the SNR for PWM in a wireless optical communication channel, taking into account pointing errors and the Gamma-Gamma distribution model for beam deflection angles of 10 and 20 degrees, as well as receiver aperture diameters of 1 mm and 2 mm. In this scenario, the average accuracy of the embedded PA system is 96.74%. Notably, this accuracy is 1% lower than that of the previous case. Table 11 shows that the maximum and minimum values of data transmission rate and accuracy in the Embedded PA System with different beam angles and receiver aperture diameters for PWM modulation in a wireless optical communication channel are influenced by pointing errors and the Gamma-Gamma distribution model.

An important factor in designing the embedded PA system is the diameter of the receiver aperture. Figure 12 illustrates the data rate values for two systems—embedded and analytical power allocation—using PWM in a wireless optical communication channel. This channel incorporates pointing errors and employs a Gamma-Gamma distribution model.

The analysis considers receiver aperture diameters of 10 mm and 15 mm, a transmitter aperture diameter of 3 mm, and a beam deflection angle of 30 degrees. In this scenario, the accuracy of the embedded PA system is 99.76%, exceeding previous cases.

Additionally, Table 12 presents the maximum and minimum data rate and accuracy values for the embedded PA system under PWM modulation, considering various beam angles and aperture diameters for both the receiver and transmitter in the wireless optical communication channel with pointing errors and a Gamma-Gamma distribution model.

In this section, the embedded PA system is evaluated in terms of BER. Figure 13 shows the BER values in terms of SNR and power budget for four modulation schemes (NRZ, RZ, PWM, and PPM) of the FSO channel with a Log-Normal distribution model in the embedded PA system. According to Table 13, the lowest BE value in this case is 0.0013.

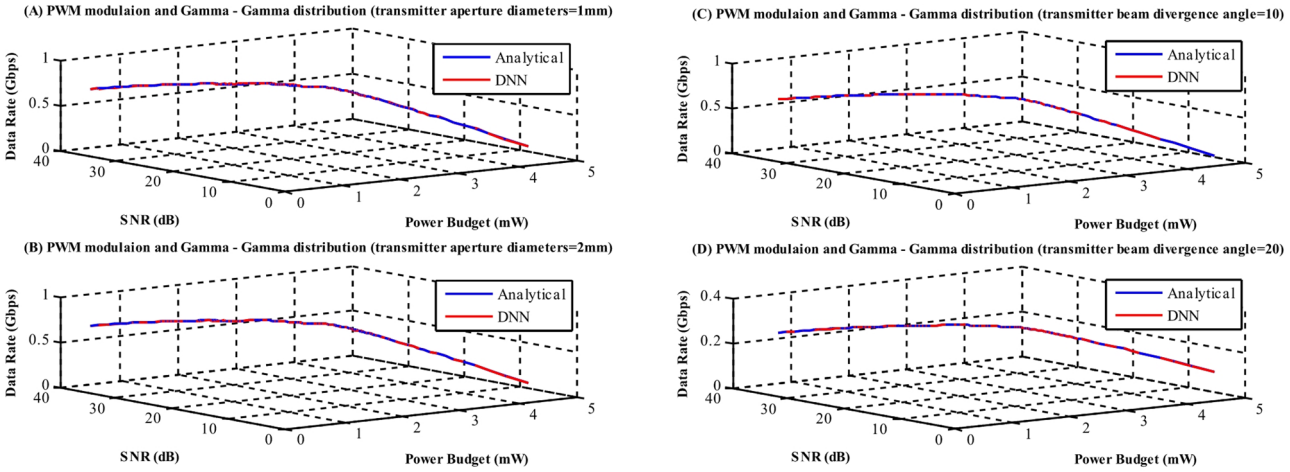

Fig. 11. The data transmission rate varies in the embedded and analytical power allocation system based on the SNR when using PWM in a wireless optical communication channel. This analysis accounts for pointing errors and utilizes a Gamma-Gamma distribution model to address beam angle deviations of 10 and 20 degrees, as well as transmitter aperture diameters of 1 mm and 2 mm.

Transmitter type	Min total power (mW)	Max total power (mW)	Min sum rate (Gbps)	Max sum rate (Gbps)	Accuracy %
Ap-Dia = 1 mm	0.4521	4.71	0.1110	0.6577	93.35
Ap-Dia = 2 mm	0.4520	4.74	0.1110	0.6580	95.72
Beam-Div = 10	0.4551	4.71	0.0741	0.6065	99.09
Beam-Div = 20	0.4599	4.72	0.0741	1.6065	98.81

Table 11. The maximum and minimum values of data transmission rate and accuracy in the embedded PA system for PWM modulation in a wireless optical communication channel are affected by pointing errors and the Gamma-Gamma distribution model. Furthermore, these values vary with different beam angles and the diameters of the receiver apertures.

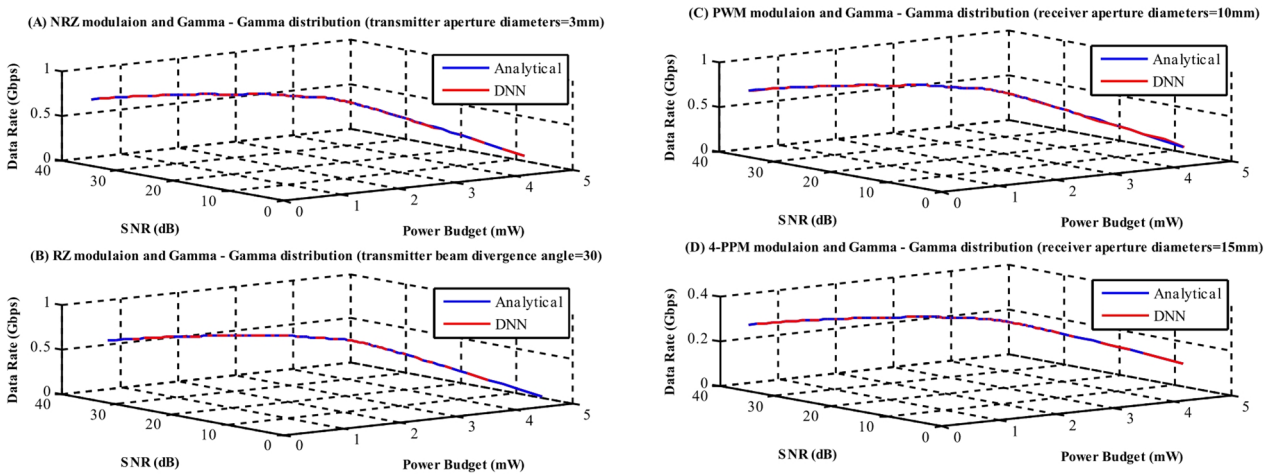

Fig. 12. The data rate values for two systems—embedded and analytical power allocation using PWM modulation are analyzed in relation to the SNR within a wireless optical communication channel. This analysis considers pointing errors and employs a Gamma-.

In this section, the performance of the embedded PA system for the FSO channel with the Gamma-Gamma distribution model is investigated. Figure 14 shows the BER values in terms of SNR and power budget for four modulation forms (NRZ, RZ, PWM, and PPM) of the FSO channel with the Gamma-Gamma distribution model in the embedded PA system.

Transmitter and receiver type	Min total power (mW)	Max Total Power (mW)	Min Data Rate (Gbps)	Max Data Rate (Gbps)	Accuracy %
Tx-Ap-Dia = 3 mm	0.4564	4.70	0.1110	0.6580	99.65
Tx- Beam-Div = 30	0.4555	4.71	0.0741	0.6065	99.82
Rx-Ap-Dia = 10 mm	0.4635	4.71	0.1110	0.6580	99.79
Rx-Ap-Dia = 15 mm	0.4697	4.75	0.1110	0.6790	99.81

Table 12. The maximum and minimum values of data transmission rate and accuracy in the embedded PA system for PWM modulation in a wireless optical communication channel are affected by pointing errors and follow a Gamma-Gamma distribution model. Additionally, these values vary with different beam angles and the aperture diameters of both the receiver and transmitter.

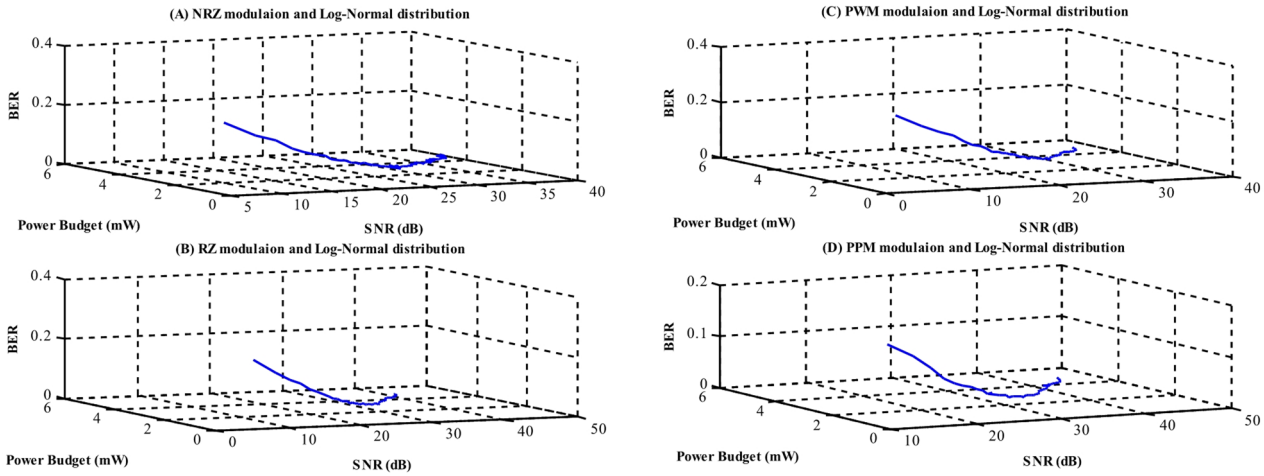

Fig. 13. BER variations based on power budget from the output of the implemented DNN model for different modulations using the Log-Normal distribution.

Modulation type	Min total power (mW)	Max total power (mW)	Min BER	Max BER
NRZ	0.4556	4.81	0.2364	0.0045
RZ	0.4551	4.72	0.2195	0.0027
PWM	0.4526	4.71	0.2699	0.0068
4-PPM	0.4530	4.73	0.1574	0.0013

Table 13. Maximum and minimum BER values, in the embedded PA system for different modulation types within the wireless optical communication channel, follow a Log-Normal distribution model.

Also, in Table 14, the maximum and minimum values for BER are reported for the transmitter power values. In this case, the BER values are significantly reduced compared to the channel with the Log-Normal distribution.

Discussion, conclusions and future work

In this paper, we present the design of an embedded optimal PA system for FSO-RF wireless communication channels, utilizing DNN alongside analytical models. Traditional analytical allocation methods tend to require extensive computational resources and processing power, making them unsuitable for communication channels that experience variable conditions. By developing a PA system based on neural networks, specifically DNNs, we can achieve the desired accuracy and speed for power management in optical-radio communication channels.

The data necessary for training the DNN were generated using established analytical algorithms. These algorithms included the WMMSE algorithm for the RF channel and BER calculations for allocating power ranges to receivers in the FSO channel. Following data normalization, we used this information to train the neural models.

We implemented two DNNs on the Jetson Nano platform, designing an embedded PA system and subsequently comparing and validating its output against benchmark algorithms. The research results indicate that the average accuracy of the embedded PA system for the RF channel is 98.49% with 10 users, 97.91% with 20 users, and 97.06% with 30 users. It was noted that the accuracy of the system decreases as the number of users increases, whereas the total data rate improves with more users.

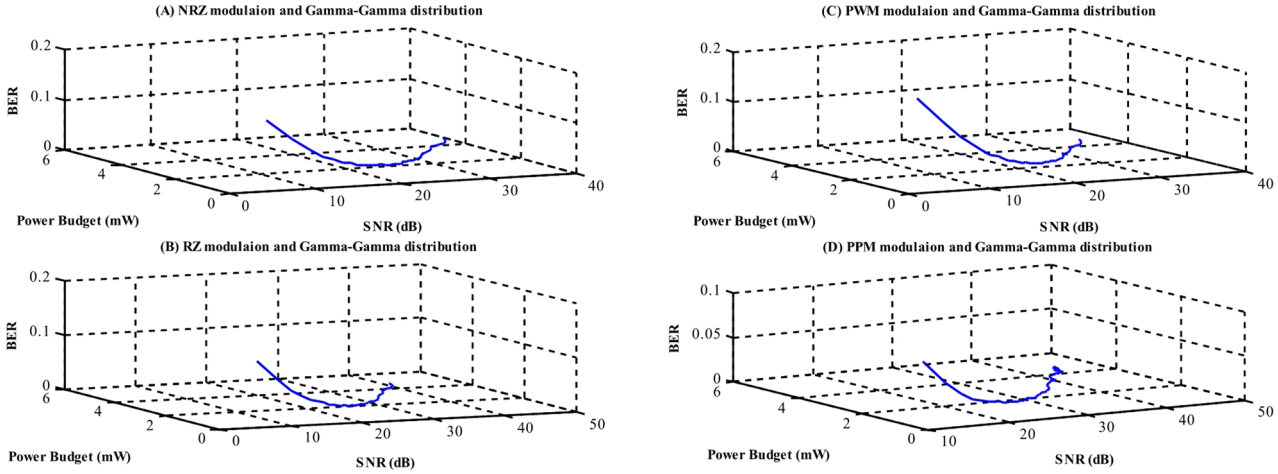

Fig. 14. BER variations based on power budget from the output of the implemented DNN model for different modulations using the Log-Normal distribution.

Modulation type	Min total power (mW)	Max total power (mW)	Min BER	Max BER
NRZ	0.4509	4.70	0.1339	3.98×10^{-4}
RZ	0.4531	4.73	0.1169	2.38×10^{-4}
PWM	0.4552	4.71	0.1845	4.43×10^{-4}
4-PPM	0.4554	4.74	0.0709	1.09×10^{-4}

Table 14. BER values in the embedded PA system for various modulations in a wireless optical communication channel are analyzed using a Gamma-Gamma distribution model.

For the FSO channel, the average accuracy of the embedded PA system was 99.29% with the Gamma-Gamma model and 99.71% with the Log-Normal model. Accuracy levels of 96.74% were observed for various transmitter aperture diameters and beam angles, and 99.76% for receivers with different aperture diameters. These findings suggest that variations in transmitter aperture diameter and beam deviation angle diminish the accuracy of the embedded PA system.

Overall, the results demonstrate that the embedded PA system designed with DNNs offers suitable accuracy and speed for managing power in FSO-RF wireless channels.

Currently, the accuracy of the RF channel is slightly lower than that of the FSO channel due to its specific characteristics such as fading and noise. To improve the accuracy of the RF channel, several approaches can be considered.

The first approach is to use deeper architectures. DNN Using deeper neural networks with more layers and more neurons in each layer can help the model better model more complex features of the RF channel such as fading and noise variations. This method can improve the accuracy of the model in more challenging conditions. Also, using ensemble learning techniques such as Random Forest or Gradient Boosting Machines can increase the accuracy of the model. These methods can help improve performance in nonlinear conditions, especially when combined with DNN models.

In future research, the system will also be able to continuously learn from new data and update DNN models incrementally through online learning. This can be especially effective in the face of sudden changes such as an increase in the number of users or changes in weather conditions, allowing the system to dynamically adapt to the new situation without the need for complete retraining.

On the other hand, if there is a need to integrate new modulations or new channel conditions, transfer learning can be used. This method enables the model to transfer features learned in different environments to new conditions using quantitative data, and it performs retraining only on specific parts of the model to reduce computational costs.

The system can also use automatic adaptation techniques to detect dynamic changes. For example, in the event of significant changes in the number of users or weather conditions affecting the FSO channel, the system can automatically adjust the model parameters. These adjustments can include adjusting the DNN hyperparameters or reducing the dimensionality of the inputs to maintain performance in the new conditions.

These approaches in future research could help the system adapt more to real-world environments and reduce the need for complete retraining.

Data availability

The original contributions presented in this study are included in the article. Further inquiries can be directed to the corresponding author.

Received: 23 August 2025; Accepted: 6 October 2025
Published online: 12 November 2025

References

1. Perdana, R. H. Y. *Deep Neural Network Design with SLNR and SINR Criterions for Downlink Power Allocation in multi-cell multi-user Massive* (MIMO systems. ICT Ex, 2022).
2. Akbari, M. & Olyaee, S. Performance analysis of total Attenuation effects and different values of transmitter power on bit error rate and Signal-to-noise ratio for free space optical communication. Recent Advances in Electrical & Electronic Engineering (Formerly Recent Patents on Electrical & Electronic Engineering), **15**(3), 234–242 (2022).
3. He, Z., Wang, L., Ye, H., Li, G. Y. & Juang, B. H. F. Resource allocation based on graph neural networks in vehicular communications. In GLOBECOM 2020–2020 IEEE Global Communications Conference, pp. 1–5. IEEE. (2020).
4. Hui, H. Intelligent Resource Allocation Method for Wireless Communication Networks Based on Deep Learning Techniques. Journal of Sensors 2021. (2021).
5. Heidari, M., Akbari, M. & Olyaee, S. Investigating and Improving the Efficiency of Space-time Codes in Visible light Communication Systems based on a Multi-input-multi-output Channel Model. Recent Advances in Electrical & Electronic Engineering (Formerly Recent Patents on Electrical & Electronic Engineering), 17(7), pp.687–697. (2024).
6. Nasir, Y. S. & Guo, D. Deep reinforcement learning for joint spectrum and power allocation in cellular networks. In 2021 IEEE Globecom Workshops (GC Wkshps), pp. 1–6. IEEE. (2021).
7. TR 21.915 v15.0.0–3rd Generation Partnership Project. Technical Specification Group Services and System Aspects; release 15 description; summary of rel-15 work items (release 15), tech. rep., 3rd Generation Partnership Project. (2019).
8. Sanguinetti, L., Zappone, A. & Debbah, M. Deep learning power allocation in massive MIMO. In 2018 52nd Asilomar conference on signals, systems, and computers, pp. 1257–1261. IEEE. (2018).
9. Sun, H. et al. Learning to optimize: training deep neural networks for interference management. *IEEE Trans. Signal Process.* **66** (20), 5438–5453 (2018).
10. Akbari, M., Olyaee, S. & Baghersalimi, G. Design and Implementation of Real-Time Optimal Power Allocation System with Neural Network in OFDM-Based Channel of Optical Wireless Communications. *Electronics*, *14*(8), p.1580. (2025).
11. Abadi, M. et al. Tensorflow: A system for large-scale machine learning, in12th USENIX Symposium on Operating Systems Design and Implementation (OSDI16), pp. 265–283. (2016).
12. Narottama, B. & Shin, S. Y. Quantum neural networks for resource allocation in wireless communications. *IEEE Trans. Wirel. Commun. Vol.* **21**, 2 (2021).
13. Jouppi, N. P. et al. In-datacenter performance analysis of a tensor processing unit, in Proc. ACM/IEEE 44th Annual International Symposium on Computer Architecture (ISCA), pp. 1–12. (2017).
14. Sun, Y., Peng, M., Zhou, Y., Huang, Y. & Mao, S. Application of machine learning in wireless networks: key techniques and open issues. *IEEE Commun. Surveys& Tutorials*. **21** (4), 3072–3108 (2019).
15. Zappone, A., Di Renzo, M. & Debbah, M. Wireless networks design in the era of deep learning: Model-based, AI-based, or both? *IEEE Trans. Commun.* **67** (10), 7331–7376 (2019).
16. Salhab, A. M., Al-Qahtani, F. S., Radaydeh, R. M., Zummo, S. A. & Alnuweiri, H. Power allocation and performance of multiuser mixed RF/FSO relay networks with opportunistic scheduling and outdated channel information. *J. Lightwave Technol.* **34** (13), 3259–3272 (2016).
17. Li, X., Li, Y., Zhao, S., Song, X. & Li, J. Performance analysis of parallel Free-Space Optical/Radio frequency transmissions in Satellite–Aerial–Ground integrated network with power allocation. In Photonics (Vol. 11, No. 12, 1162). MDPI. (2024).
18. Zwaid Alsulami, O. et al. Resource Allocation in Co-existing Optical Wireless HetNets. arXiv e-prints, pp.arXiv-2004. (2020).
19. Sun, H. et al. June. Learning to continuously optimize wireless resource in episodically dynamic environment. In ICASSP 2021–2021 IEEE International Conference on Acoustics, Speech and Signal Processing (ICASSP) (pp. 4945–4949). IEEE. (2021).
20. Alazwary, K. D., Qidan, A. A., El-Gorashi, T. E. H. & Elmirghani, J. M. Deep Learning-based power allocation in rate splitting optical wireless networks. (2023). arXiv preprint arXiv:2307.08399.
21. Li, Y., Geng, T., Tian, R. & Gao, S. Power allocation in a spatial multiplexing free-space optical system with reinforcement learning. Optics Communications, 488, p.126856. (2021).
22. Aletri, O. Z. et al. Optimum resource allocation in optical wireless systems with energy-efficient fog and cloud architectures. Philosophical Transactions of the Royal Society A, 378(2169), p.20190188. (2020).
23. Khadmaoui-Bichouna, M., Escolar, A. M., Alcaraz-Calero, J. M. & Wang, Q. Design and implementation of an integrated OWC and RF network slicing-based architecture over hybrid LiFi and 5G networks. *Wireless Netw.* **31** (2), 1541–1559 (2025).
24. Shi, S., Li, G., An, K., Gao, B. & Zheng, G. Energy-efficient optimal power allocation in integrated wireless sensor and cognitive satellite terrestrial networks. Sensors, 17(9), p.2025. (2017).
25. Enayati, S., Saeedi, H. & Mokari, N. September. Throughput maximization in hybrid FSO/RF communication systems. In 2015 4th International Workshop on Optical Wireless Communications (IWOW) (pp. 51–54). IEEE. (2015).
26. Ben Halima, N. & Boujemaa, H. Optimal power allocation and harvesting duration for mixed RF/FSO using non orthogonal multiple access. Optical and Quantum Electronics, 52(10), p.442. (2020).
27. Youssef, R. et al. Hybrid FSO/RF communications system demonstrated across degraded 30 Km link with integrated commercial radio. In Free-Space Laser Communications XXXVI (Vol. 12877, 191–199). SPIE. (2024).
28. Ali Amirabadi, M. & Tabataba Vakili, V. Performance analysis of a novel hybrid FSO/RF communication system. *IET Optoelectron.* **14** (2), 66–74 (2020).
29. Bopardikar, R., Joseph, C. & Raj, A. B. A review paper on hybrid RF/FSO system for communication. *Int. J. Eng. Res. Reviews*, **12**(3), pp.90–115 https://doi.org/10.5281/zenodo.13848040 (2024).
30. Li, X., Li, Y., Song, X., Li, J. & Zhao, S. Diversity scheme based hybrid FSO/RF systems in satellite-aerial-ground integrated network with outdated CSI. *Scientific Reports*, *15*(1), p.26344 (2025).
31. Adardour, H. E. & Kameche, S. Performance analysis of free space optical networks using the beta-average recursive estimator. *Wireless Pers. Commun.* **114** (3), 2717–2732 (2020).
32. Adardour, H. E., Kameche, S. & Singh, M. A MIMO-Enabled Free Space Optical Link under Log-Normal Fading/Gamma-Gamma Channel: Exploring an Optimal Modulation Scheme. *International Journal of Optics*, *2023*(1), p.8020925. (2023).
33. Derouiche, S., Kameche, S. & Adardour, H. E. 5G network performance using novel MIMO mixed FSO/MMW communication systems under pointing errors effect: Test analysis using image transmission. *Journal of Optics*, *26*(11), p.115707. (2024).
34. Hayle, S. T. et al. High-speed FSO-5G wireless communication system with enhanced loss compensation using high-power EDFA. *Scientific Reports*, *15*(1), p.379. (2025).
35. Proakis, J. G. & Salehi, M. *Digital Communications* (McGraw-hill, 2008).
36. Haykin, S. *Communication Systems* (Wiley, 2008).

37. Anis, A. A., Rashidi, C. B. M., Rahman, A. K., Aljunid, S. A. & Ali, N. Analysis of the effect of BER and Q-factor on free space optical communication system using diverse wavelength technique. In EPJ Web of Conferences, vol. 162, p. 01024. EDP Sciences, (2017).
38. Basudewa, M. I., Bagaskara, Z. H., Damita, S. S. A., Putra, R. F. & Ahmadi, D. Bit error rate performance analysis for free space optic communication. In IOP Conference Series: Materials Science and Engineering, vol. 850, no. 1, p. 012056. IOP Publishing, (2020).
39. Alnajjar, S. H., Ammar, A., Noori & Arwa, A. Moosa. Enhancement of FSO communications links under complex environment. *Photonic Sens.* **7** (2), 113–122 (2017).
40. Akbari, M. & Olyaee, S. BER performance analysis in SISO and MIMO-FSO channels with pointing error and different models. *Int. J. Electron.*, pp.1–21. https://doi.org/10.1080/00207217.2025.2501290 (2025).
41. Rappaport, T. S. *Wireless Communications: Principles and practice, 2/E* (Pearson Education India, 2010).
42. Shi, Q., Razaviyayn, M., Luo, Z. Q. & He, C. An iteratively weighted MMSE approach to distributed sum-utility maximization for a MIMO interfering broadcast channel. *IEEE Trans. Signal Process.* **59** (9), 4331–4340 (2011).
43. Yang, H. et al. Knowledge-driven resource allocation for wireless networks: A WMMSE unrolled graph neural network approach. *IEEE Internet Things J.* **11** (10), 18902–18916 (2024).

Acknowledgements
This work was supported by the Nano-photonics and Optoelectronics Research Laboratory (NORLab), Shahid Rajaee Teacher Training University, and ICT Research Institute (IRAN Telecommunication Research Center (ITRC)) under Project No 14403.

Author contributions
M.A. designed and performed simulations, analyzed data, and drafted the manuscript. S.O. supervised, verified, reviewed, and edited the manuscript. G.B. verified and edited the manuscript. All authors read and approved the final manuscript.

Funding
This work was supported by the Shahid Rajaee Teacher Training University under grant number 1404/388038.

Declarations

Competing interests
The authors declare no competing interests.

Additional information
Correspondence and requests for materials should be addressed to S.O.